

Anomalous metallic state and anisotropic multiband superconductivity in $\text{Nb}_3\text{Pd}_{0.7}\text{Se}_7$

Q. Zhang,¹ D. Rhodes,¹ B. Zeng,¹ T. Besara,¹ T. Siegrist,^{1,2} M. D. Johannes,³ and L. Balicas^{1,*}

¹*National High Magnetic Field Laboratory, Florida State University, Tallahassee-FL 32310, USA*

²*Department of Chemical and Biomedical Engineering,
Florida State University, Tallahassee, Florida 32310, USA.*

³*Center for Computational Materials Science, Naval Research Laboratory, Washington, DC 20375, USA*

(Dated: June 22, 2021)

We report the discovery of superconductivity in $\text{Nb}_3\text{Pd}_x\text{Se}_7$ with a x -dependent superconducting transition-temperature as high as $T_c \simeq 2.1$ K for $x \simeq 0.7$ (middle point of the resistive transition). Needle-like single crystals display anisotropic upper-critical fields with an anisotropy $\gamma = H_{c2}^b/H_{c2}^a$ as large as 6 between fields applied along their needle axis (or b -axis) or along the a -axis. As for the Fe based superconductors γ is temperature-dependent suggesting that $\text{Nb}_3\text{Pd}_{0.7}\text{Se}_7$ is a multi-band superconductor. This is supported by band structure calculations which reveal a Fermi surface composed of quasi-one-dimensional and quasi-two-dimensional sheets of hole character, as well as three-dimensional sheets of both hole- and electron-character. Remarkably, H_{c2}^b is observed to saturate at $H_{c2}^b(T \rightarrow 0\text{K}) \simeq 14.1$ T which is $4.26 \times H_p$ where H_p is the Pauli-limiting field in the weak-coupling regime. The synthesis procedure yields additional crystals belonging to the $\text{Nb}_2\text{Pd}_x\text{Se}_5$ phase which also becomes superconducting when the fraction of Pd is varied. For both phases we find that superconductivity condenses out of an anomalous metallic state, i.e. displaying $\partial\rho/\partial T < 0$ above T_c similarly to what is observed in the pseudogap-phase of the underdoped cuprates. An anomalous metallic state, low-dimensionality, multi-band character, extremely high and anisotropic H_{c2} s, are all ingredients for unconventional superconductivity.

INTRODUCTION

The Fe chalcogenide compounds, such as $\text{Fe}_{1+\delta}\text{Se}$, $\text{Fe}_{1+\delta}\text{Se}_x\text{Te}_{1-x}$, or the $A_x\text{Fe}_{2-y}\text{Se}_2$ ($A = \text{Tl}, \text{Rb}$ or K) display remarkable superconducting properties. For example, the tetragonal phase of $\text{Fe}_{1+\delta}\text{Se}$ (i.e. when $0.01 \leq \delta \leq 0.04$) displays superconductivity at $T_c \sim 8.5$ K only when $\delta = 0.01$ [1], although it was recently shown that intercalation with $\text{Li}_x(\text{NH}_2)_y(\text{NH}_3)_{1-y}$ or K leads to a dramatic enhancement in T_c up to 43 K [2] and 44 K [3], respectively. For the $\text{Fe}_{1+\delta}\text{Se}_x\text{Te}_{1-x}$ series, recent angle resolved photoemission studies suggest a ratio for the superconducting gap to the Fermi energy $\Delta/\varepsilon_F \approx 0.5$ placing this system at the BCS to BEC crossover, or equivalently, that these are very strongly coupled superconductors [4]. Finally, the $A_x\text{Fe}_{2-y}\text{Se}_2$ is claimed to be close to an orbital-dependent Mott transition [5] indicating a certain resemblance with the cuprates, although several studies support the microscopic coexistence of superconductivity with magnetism and concomitant insulating states [6].

Recently, we reported the discovery of yet a new transition-metal based anisotropic multi-band superconductor, i.e. $\text{Nb}_2\text{Pd}_{0.81}\text{S}_5$, which displays extremely large upper critical fields [7]. In contrast to the Fe chalcogenides, this compound crystallizes in the lower symmetry space-group $C2/m$ which, according to band structure calculations, leads to a complex Fermi surface (FS) composed of both two-dimensional (2D) and quasi-one-dimensional (Q1D) sheets. The Pd stoichiometry is predicted to play a major role since the calculations indicate that it displaces the Fermi-level favoring nesting among the Q1D FS-sheets for particular wave-vectors, and this

would lead to electronic instabilities and possibly to itinerant magnetism [7]. Therefore, the Pd fraction is expected to play a role similar to that of F or Co and K in the “1111” and “122” Fe-arsenides respectively, [8–10] where variations in their stoichiometry is observed to induce superconductivity or increase the superconducting transition temperature in detriment of antiferromagnetism.

Given its composition and electronic anisotropy, one could expect $\text{Nb}_2\text{Pd}_{0.81}\text{S}_5$ to display physical similarities with transition-metal dichalcogenides such as $2H\text{-NbS}_2$ or $1T\text{-TaS}_2$, or some of the transition metal trichalcogenides as NbSe_3 . The former two compounds display a charge-density wave (CDW) transition followed by superconductivity at lower temperatures [11, 12]. While the latter displays two transitions towards CDW-phases upon cooling [13]. However, we did not detect any sharp anomaly that could indicate a transition akin to a Peierls instability in $\text{Nb}_2\text{Pd}_{0.81}\text{S}_5$, hence we have no evidence for the coexistence of superconductivity with a density-wave like state which is claimed to enhance the superconducting upper-critical fields (H_{c2}) in the aforementioned compounds [14]. Furthermore, and despite the similar values of T_c , $\text{Nb}_2\text{Pd}_{0.81}\text{S}_5$ displays remarkably larger H_{c2} s (by a factor of two or more depending on orientation) when compared to either NbS_2 [15] or NbSe_2 [16] and, in contrast to both compounds, it also displays a clear concave down curvature in $H_{c2}(T)$ for $H \parallel b$ -axis. These observations, indicate few similarities between $\text{Nb}_2\text{Pd}_{0.81}\text{S}_5$ and the dichalcogenide or trichalcogenide compounds. In addition, as we will see below, the properties of the metallic state of new compounds emerging from $\text{Nb}_2\text{Pd}_{0.81}\text{S}_5$ by replacing S with Se are non-Fermi liquid like in the

region of temperatures just above T_c in contrast to the aforementioned compounds. This behavior is very prominent in a very narrow range of values for the fraction x of Pd, or when $0.67 \leq x \leq 0.71$, where one observes the emergence of superconductivity from the non-superconducting compounds.

In this manuscript, we show that new families of compounds can be created by varying the chemistry of $\text{Nb}_2\text{Pd}_{0.81}\text{S}_5$, leading to new superconducting compounds such as $\text{Nb}_2\text{Pd}_x\text{Se}_5$ and $\text{Nb}_3\text{Pd}_x\text{Se}_7$. It turns out, as shown below, that $\text{Nb}_2\text{Pd}_x\text{Se}_5$ for $x \simeq 0.7$ displays a crossover from metallic ($\partial\rho/\partial T > 0$) to “non-metallic” ($\partial\rho/\partial T < 0$) upon cooling, therefore we show that superconductivity in this compound emerges from an anomalous metallic state upon cooling. This crossover like temperature is observed to decrease as T_c increases (upon variation of x), with the metallic state displaying non-Fermi liquid behavior as a function of the temperature, i.e. $\rho = \rho_0 + AT^n$ with n ranging from ~ 1 to ~ 0.4 . In contrast, the $\text{Nb}_3\text{Pd}_{0.7}\text{Se}_7$ compound, with a middle point superconducting transition temperature $T_c \simeq 2.1$ K, do display Fermi-liquid like metallic behavior (or $n = 2$) above 150 K. Nevertheless a mild anomaly centered around 110 K is observed in the resistivity, suggesting also a crossover or perhaps an electronic instability. Although in this compound T_c increases with x or the Pd content, the position of this anomaly remains unaffected by it. Similarly to the $\text{Nb}_2\text{Pd}_x\text{Se}_5$ compounds, superconductivity in the $\text{Nb}_3\text{Pd}_x\text{Se}_7$ series also emerges from a state displaying “non-metallic” character (or $\partial\rho/\partial T < 0$).

For these new chalcogenides, low dimensionality, multi-band effects, anomalous metallic behavior, and as will be discussed below for the case of $\text{Nb}_3\text{Pd}_{0.7}\text{Se}_7$, anisotropic and extremely high upper critical fields, suggest an unconventional superconducting state. Here, we focus on the superconducting phase-diagram of $\text{Nb}_3\text{Pd}_{0.7}\text{Se}_7$. A detailed account on the dependence of the superconducting phase-diagrams of $\text{Nb}_2\text{Pd}_x\text{Se}_5$ and $\text{Nb}_3\text{Pd}_x\text{Se}_7$ on x or the Pd content, will be given elsewhere.

EXPERIMENTAL

$\text{Nb}_3\text{Pd}_{0.7}\text{Se}_7$ was grown via a solid state reaction under an Ar atmosphere: Nb (99.99 %), Pd (99.99 %), and Se (99.999 %) well mixed powders in the ratio of 4:1:10 were heated to a peak temperature of 850 °C at a rate of 100 °C/h in sealed quartz ampoules, kept for 48 hours and subsequently quenched to room temperature. The obtained single crystals formed thin long needles several millimeters in length, but with cross-sectional areas ranging from $1 \times 5 \mu\text{m}^2$ up to $20 \times 100 \mu\text{m}^2$. The stoichiometric composition was determined by energy dispersive X-ray spectroscopy and single-crystal X-ray structure refinement. Two distinct crystallographic

phases were identified as resulting from the growth conditions, namely $\text{Nb}_3\text{Pd}_x\text{Se}_7$ and $\text{Nb}_2\text{Pd}_x\text{Se}_5$, with $0.67 \leq x \leq 0.701$ showing superconducting transition temperatures T_c ranging from $T_c < 0.3$ K up to ~ 2.0 and ~ 1.0 K, respectively. The detailed results of our refinements, including the respective atomic positions for typical single-crystals of each phase is given in Appendix A. A conventional four terminal configuration was used for the resistivity measurements which were performed under magnetic-field either by using a Physical Parameter Measurements System (also for heat capacity measurements) or a superconducting magnet coupled to a dilution refrigerator.

Figures 1 (a) to (d) shows the resistivity ρ normalized by its value at room temperature, i.e. $\rho/\rho(T = 300\text{K})$ as a function of the temperature (in a logarithmic scale) for five single-crystals resulting from the same synthesis process. These crystals were analyzed through single-crystal X-ray diffraction measurements to reveal both their composition and their crystallographic structure. Traces in Figs. 1 (a) and (b) were obtained from crystals belonging to the $\text{Nb}_3\text{Pd}_x\text{Se}_7$ phase, whose Pd content x was refined as $x = 0.676(2)$ (blue trace), $x = 0.68(1)$ (green trace), and $x = 0.7025(22)$ (grey trace), respectively. The room temperature resistivity of these crystals was found to oscillate between several tenths of $\mu\Omega\text{cm}$ to a few hundreds of $\mu\Omega\text{cm}$. This variability in the actual values of the resistivity can be attributed to the error bars in the determination of their geometrical factors, particularly their thickness which, for example, is approximately $1 \mu\text{m}$ for the superconducting single-crystal shown in Figs. 1 (a) and (b). As seen in the inset of Fig. 1 (a), a broad anomaly is observed in the resistivity around $T = 100$ K, indicating either an electronic phase-transition akin to a spin-density wave state seen in the Fe-pnictide superconductors [18] or a crossover towards a new electronic regime, such as the pseudogap observed in the cuprates [19]. Notice also that just above the superconducting transition ρ displays an uncharacteristic T -dependence for a metal, i.e. with a negative $\partial\rho/\partial T$, indicating the existence of a prominent quasi-particle scattering mechanism. Red lines are fits to the power law $\rho = \rho_0 + AT^n$ which yields exponents n ranging from 3.7 for the non-superconducting sample, to 2 for the superconducting one, thus suggesting that the superconducting sample displays Fermi-liquid behavior already at high temperatures. The higher exponents for the non-superconducting samples result from the pronounced upturn in the resistivity observed around 110 K. The overall behavior seen in Figs. 1 (a) and (b), i.e. a pronounced change in slope at higher temperatures followed by an uncharacteristic “non-metallic” like behavior at lower temperatures, is remarkably similar to what is seen in the underdoped regime of, for example, $\text{La}_{2-x}\text{Sr}_x\text{CuO}_4$ [20], although the resistivity in those compounds follows a linear dependence on temperature at higher temperatures.

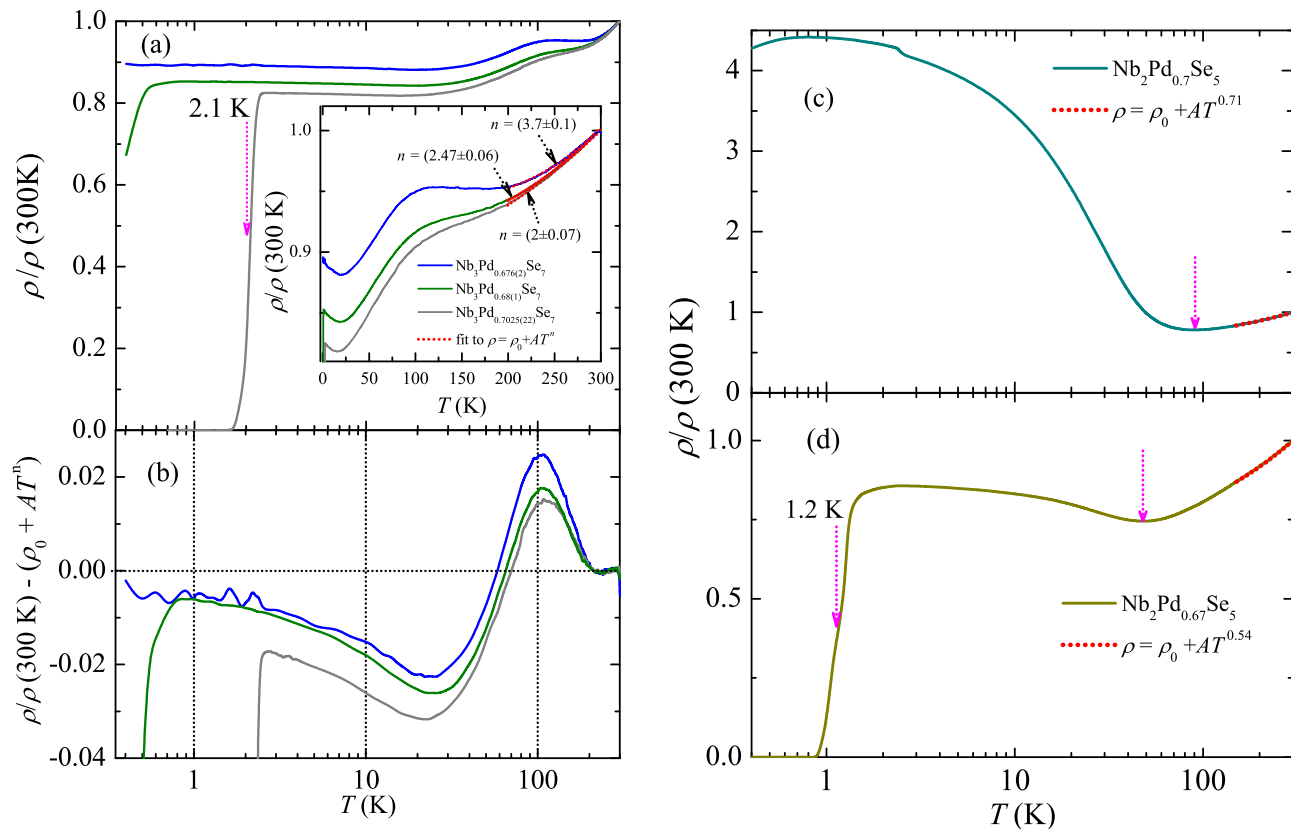


FIG. 1. (color online) (a) Resistivity ρ normalized by its value at room temperature $\rho(300\text{K})$ as a function of the temperature T for three $\text{Nb}_3\text{Pd}_x\text{Se}_7$ single-crystals, i.e. $x = 0.676(2)$ (blue line), $0.68(1)$ (green line), and $\simeq 0.7$ (grey line), respectively. The dimensions of the superconducting crystal are $\sim 1 \times 10^{-4} \times 8.5 \times 10^{-3} \times 0.2 \text{ cm}^{-3}$, leading to a room temperature resistivity of $\sim 70 \mu\Omega\text{cm}$ (for a contacts separation of $\sim 0.05 \text{ cm}$). Inset: $\rho/\rho(300\text{K})$ as a function of T in a linear temperature scale. Red lines are fits to the power law $\rho = \rho_0 + AT^n$ within the range $150 \leq T \leq 300 \text{ K}$. The superconducting compound displays Fermi-liquid like behavior or $n = 2$. (b) $\rho/\rho(300\text{K})$ after subtraction of the aforementioned power law. Notice a sharp anomaly at $T^* \sim 110 \text{ K}$ which is independent on the Pd content x , but whose amplitude is seen to decrease as x increases. This anomaly, of unknown origin is followed by a minimum in the resistivity at $T_{\min} \sim 24 \text{ K}$ suggesting electronic localization preceding the superconducting transition. (c) and (d) Resistivity $\rho/\rho(300\text{K})$ as a function of the temperature T for two $\text{Nb}_2\text{Pd}_x\text{Se}_5$ single-crystals, i.e. $x = 0.7$ and 0.67 , respectively. Notice the observation of an upturn in the resistivity at a Pd-dependent temperature, indicating again an interplay with some form of electron localization. The characteristic temperature T_{\min} below which ρ becomes “non-metallic”, decreases as the Pd content decreases. The dimensions of the $\text{Nb}_2\text{Pd}_{0.67}\text{Se}_5$ single-crystal are $\sim 1.75 \times 10^{-4} \times 3.4 \times 10^{-3} \times 0.235 \text{ cm}^{-3}$, leading to a room temperature resistivity of $\sim 225 \mu\Omega\text{cm}$. Red lines are fits to the power-law behavior observed in the metallic state, which yield non-Fermi liquid like exponents n ranging from ~ 1 (non-superconducting) to ~ 0.4 (in superconducting samples).

Figures 1 (c) and (d) show $\rho/\rho(T = 300\text{K})$ for two $\text{Nb}_2\text{Pd}_x\text{Se}_5$ single crystals, i.e. respectively for $x = 0.7$ and $x = 0.67$ resulting from the same synthesis process. Notice the pronounced but progressive increase in resistivity below $\sim 100 \text{ K}$ for the $x = 0.7$ sample, suggesting again a continuous or second-order like electronic phase-transition or perhaps a crossover towards a pseudogap-like regime. Therefore, for *both* compounds $x = 0.7$ defines a threshold concentration separating superconducting from non-superconducting samples. Remarkably, while the increase in x beyond 0.7 induces superconductivity in $\text{Nb}_3\text{Pd}_x\text{Se}_7$ it is observed to *suppress* superconductivity in $\text{Nb}_2\text{Pd}_x\text{Se}_5$. This suggests that su-

perconductivity is stabilized by small displacements of the Fermi level, or equivalently that in both compounds the Fermi level is located in close proximity to a van Hove singularity. For the $\text{Nb}_2\text{Pd}_x\text{Se}_5$ compounds, we found that the exponent in the power law describing ρ at high temperatures ($150 \text{ K} \leq T \leq 300 \text{ K}$) evolves from a value close to 1 when $x \sim 0.7$, to $n \sim 0.5$ in the superconducting samples (or when $x \simeq 0.67$) which corresponds to non-Fermi liquid behavior, and cannot be easily ascribed to scattering by phonons. Furthermore, the superconducting transition for $\text{Nb}_2\text{Pd}_{0.67}\text{Se}_5$ is preceded by an upturn in the resistivity starting at $T = 48 \text{ K}$. Therefore, for both compounds and for $0.67 \leq x \lesssim 0.7$ superconduc-

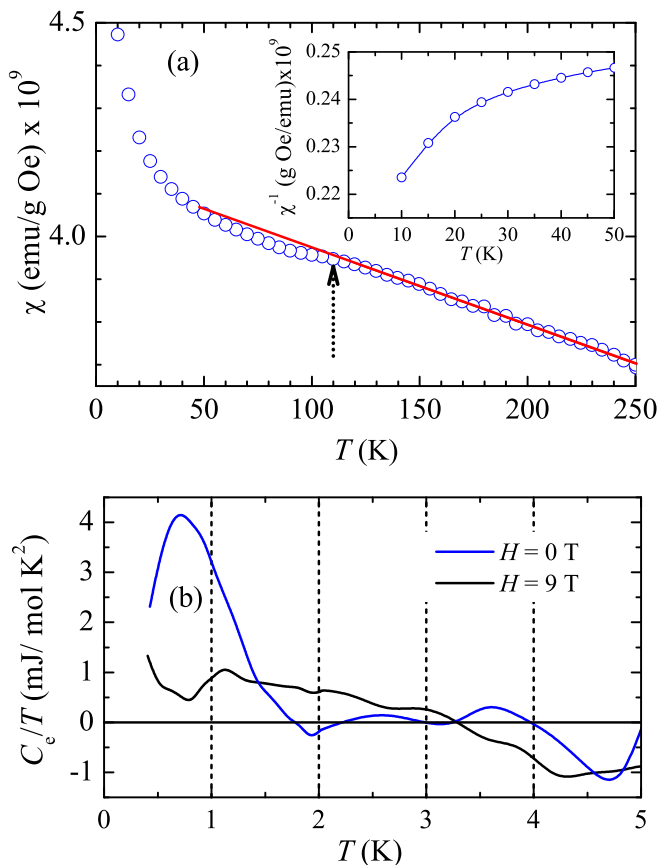


FIG. 2. (color online) Heat capacity normalized by T and as a function of T for hundreds of single-crystals from a typical synthesis batch, which contains both phases. One observes a broad anomaly centered around $T = 0.75$ K, which disappears with the application of a field of 9 T, indicating bulk superconductivity.

tivity condenses out of an unconventional metallic state.

As discussed below as well as in Ref. 7, the geometry of the FS of these compounds is complex and contains quasi-one-dimensional sheets which are the necessary ingredient for a Peierls-like instability which could lead to itinerant magnetism. The broad anomaly seen around 110 K in $\text{Nb}_3\text{Pd}_{0.7}\text{Se}_7$ single-crystals could correspond to evidence for such a transition and therefore in Fig. 2 (a) we show the magnetic susceptibility χ as a function of the temperature for a batch containing hundreds of randomly oriented single-crystals. We used hundreds of crystals, given that a typical individual single-crystal, whose data are shown above, weights only $\sim 1 \mu\text{g}$. We found that this particular batch is composed almost exclusively of crystals belonging to the $\text{Nb}_3\text{Pd}_x\text{Se}_7$ phase. As seen, at higher temperatures $\chi(T)$ varies little showing an unexpected linear dependence in temperature which could be an indication for Pauli-like susceptibility, but with a temperature-dependent density of states at the Fermi level. Around 110 K one observes just a mild deviation

from linearity as indicated by the arrow, hence it does not represent a clear evidence for an electronic or magnetic phase-transition. For $T < 50$ K, $\chi(T)$ displays a sharp upturn which, as seen in the inset, does not correspond to a Curie tail: the inset plots the inverse of $\chi(T)$ in a limited temperature, i.e. for $T < 50$ K, and as seen it is not linear in temperature. Consequently, this upturn cannot be attributed to the presence of impurities and most likely corresponds to evidence for magnetic correlations. A fit to a power law yields a very small exponent suggesting a $\log -T$ divergence. Fig. 2 (b), on the other hand, shows the electronic contribution to the heat capacity C_e normalized by the temperature T , after the subtraction of a T^3 term and for two values of the field, respectively $H = 0$ and 9 T. Again, hundreds of single-crystals from one synthesis batch (~ 2 mg), therefore of varying stoichiometry, were used for these measurements. A broad anomaly in C_e/T emerges below ~ 1.5 K and peaks at ~ 0.7 K, with its width determined by the distribution of T_c s, as seen in the upper panel. This anomaly is suppressed by the application of an external magnetic-field, as expected for bulk superconductivity. Therefore, our observations clearly indicate bulk superconductivity. We emphasize that the data shown in Fig. 1 corresponds to crystals displaying among the highest T_c s within the batches synthesized by us. In contrast, the heat capacity yields an average value for T_c .

$\text{Nb}_3\text{Pd}_{0.7}\text{Se}_7$ crystallizes in the space group $C2/m$ (see Fig. 3) and can be described as composed of sheets of a single $\text{Nb}_6\text{PdSe}_{14}$ basic unit which is comprised of chains formed by square-planar and trigonal-prismatic Se polyhedra which are approximately centered by Pd and Nb atoms, respectively (see Ref. 17). Each chain extends along the $[010]$ direction (needle axis). The Pd(1) atoms center a column of face-to-face square planes. Both Nb(1) and Nb(2) atoms occupy chains of edge-sharing trigonal prisms while the Nb(3) atoms occupy columns of face sharing trigonal prisms. The basic $\text{Nb}_6\text{PdSe}_{14}$ is formed in such a way that the polyhedra in adjacent columns share their edges. The $\text{Nb}_6\text{PdSe}_{14}$ layers form via interdigitation of the $\text{Nb}_6\text{PdSe}_{14}$ units, with the Nb(3) atoms acquiring a seven-coordinate, monocapped trigonal-prismatic environment. The three-dimensional structure results from the stacking of these layers in a closed packed (Se atoms) fashion. The Pd(2) atom occupies a rhombic site between the layers and is square-planar coordinated with the Se(1) atoms.

Given the low crystallographic symmetry of $\text{Nb}_3\text{Pd}_{0.7}\text{Se}_7$ one expects an anisotropic response for magnetic fields applied along its distinct crystallographic axis. Therefore, we show the resistivity of a second $\text{Nb}_3\text{Pd}_{0.7}\text{Se}_7$ single-crystal ($T_c \simeq 1.8$ K) for several temperatures and as a function of the magnetic-field H applied along the a - and the c -axis (Figs. 4 (a) and 4 (b), respectively) and for fields along the b - or the needle-axis (Fig. 4 (c)). This crystal was placed

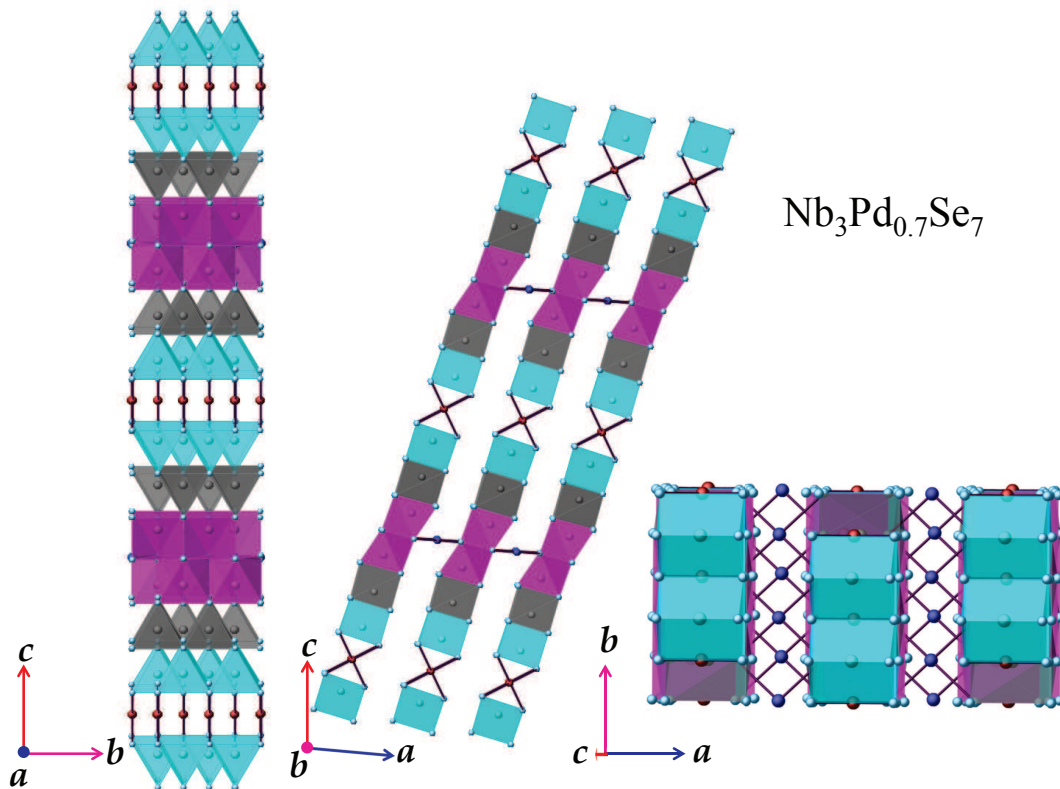


FIG. 3. (color online) (a) From left to right, distinct perspectives of the crystallographic structure of $\text{Nb}_3\text{Pd}_{0.7}\text{Se}_7$: along the a -, b -, and nearly along the c -axis, respectively. The Nb(1), Nb(2), and Nb(3) atoms are depicted in turquoise, grey, and magenta colors, respectively. Pd(1) and Pd(2) atoms are depicted in maroon and dark blue colors, whereas all the Se atoms are depicted in clear blue color, respectively.

onto a sapphire substrate and the external field was initially applied perpendicularly to (b, c) -plane (Fig. 4 (a)). Subsequently, the field was rotated by 90° with respect to this previous orientation, while remaining perpendicular to needle-axis (Fig. 4 (b)). Subsequently, it was rotated by 90° around the c -axis in order to align the field along the b -axis (Fig. 4 (c)). As seen, the resistive transitions from the superconducting to the metallic state for the different field orientations reveal rather anisotropic upper-critical fields H_{c2} .

DISCUSSION

In Figure 5, we display the resulting $H_{c2} - T$ phase-diagram, constructed by plotting the middle point of the resistive transitions shown in Fig. 4 as well as from the resistivity as a function of T under field (not shown). Remarkably, H_{c2} for fields along the b -axis saturates at a value of $H_{c2}(T \rightarrow 0 \text{ K}) \sim 14.1 \text{ T}$ which is $4.26 \times H_p [= 1.84T_c (\simeq 1.8 \text{ K})]$, where H_p is the Pauli limiting field in the weak coupling regime. To put this value in perspective, compare the ratio $H_{c2}(T \rightarrow 0 \text{ K})/T_c = 14.1 \text{ T}/1.8 \text{ K} = 7.83$ with the corresponding ratios for

$\text{Fe}_{1+y}\text{Se}_{0.45}\text{Te}_{0.55}$, ($\sim 50 \text{ T}/14 \text{ K} \simeq 3.57$) [21], CeCoIn_5 ($\sim 12 \text{ T}/2.3 \text{ K} = 5.2$) [22], URu_2Si_2 ($\sim 12.5 \text{ T}/1.5 \text{ K} = 8.33$) [23] which, according to all evidence, are unconventional and strongly-correlated superconductors. Notice that this ratio for $\text{Nb}_3\text{Pd}_{0.7}\text{Se}_5$ also surpasses the respective one for $\text{Nb}_2\text{Pd}_{0.81}\text{S}_5$ ($\sim 37 \text{ T}/6.6 \text{ K} \simeq 5.6$) [7], or for the Chevrel-phase PbMo_6S_8 ($\sim 60 \text{ T}/13.3 \text{ K} \simeq 4.51$) [24], and obviously the ratio for the widely used Nb_3Sn compound ($\sim 30 \text{ T}/18 \text{ K} \simeq 1.67$) [25]. Finally, and although the anisotropy γ for $\text{Nb}_3\text{Pd}_{0.7}\text{Se}_7$ is not as high as the one reported for $\text{Li}_{0.9}\text{Mo}_6\text{O}_{17}$, which suggests that this later compound is considerably more quasi-one-dimensional [26], its ratio $H_{c2}(T \rightarrow 0 \text{ K})/T_c \sim 15 \text{ T}/2.2 \text{ K} = 6.82$ still is smaller than the ratio reported here.

Below we show Ginzburg-Landau fittings of the phase-boundary, which for fields along the b -axis yields an orbital limiting field $H_0 = (35 \pm 3) \text{ T}$ and $H_p = (19 \pm 1) \text{ T}$, therefore suggesting that $\text{Nb}_3\text{Pd}_{0.7}\text{Se}_7$ could be a Pauli limited superconductor displaying a very large Maki parameter $\alpha = \sqrt{2}H_0/H_p = 2.6$ if one uses both field values resulting from the fittings, or $\alpha \simeq 3.5$ if one uses the actual experimental result 14.1 T . In any case, these values for α are > 1.8 the value required for the observation of the Fulde-Ferrel-Larkin-Ovchinnikov-state [27]. Below

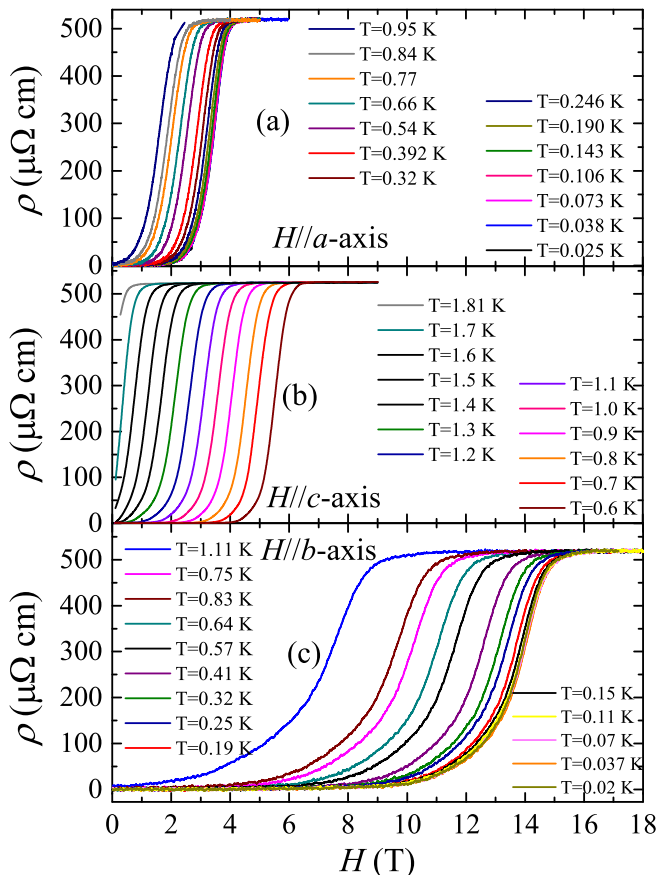


FIG. 4. (color online) (a) Resistivity ρ as a function of the field H applied along the a -axis of a $\text{Nb}_3\text{Pd}_{0.7}\text{Se}_7$ single-crystal for several temperatures. (b) Same as in (a) but fields along the c -axis and at pumped ^3He temperatures. (c) Same as in (a) but for fields along the b -axis.

we also show a fit of $H_{c2}^b(T)$ to the Werthamer-Helfand-Hohenberg formalism [29], indicating that a large α value of ~ 2.4 would fit the boundary, but would require a large spin-orbit coupling implying that this coupling is relevant for this system. Finally, as seen in the lower panel of Fig. 4, the superconducting anisotropy $\gamma = H_{c2}^b/H_{c2}^a$ is T -dependent as seen in the Fe pnictides/chalcogenides and interpreted as evidence for multi-band effects [30, 31].

In order to evaluate the contributions of both orbital and Pauli pair-breaking effects for all field orientations we analyze our $H_{c2}(T)$ data at temperatures close to T_c where the Ginzburg-Landau (GL) theory yields [28]:

$$\left(\frac{H}{H_p}\right)^2 + \frac{H}{H_o} = 1 - \frac{T}{T_c} \quad (1)$$

Very close to the critical temperature, $(T_c - T)/T_c \ll (H_p/H_o)^2$, the first paramagnetic term in the left hand side is negligible and Eq. (1) yields the orbital linear Ginzburg-Landau temperature dependence, $H_{c2} = H_o(1 - T/T_c)$. At lower temperatures, $(T_c - T)/T_c >$

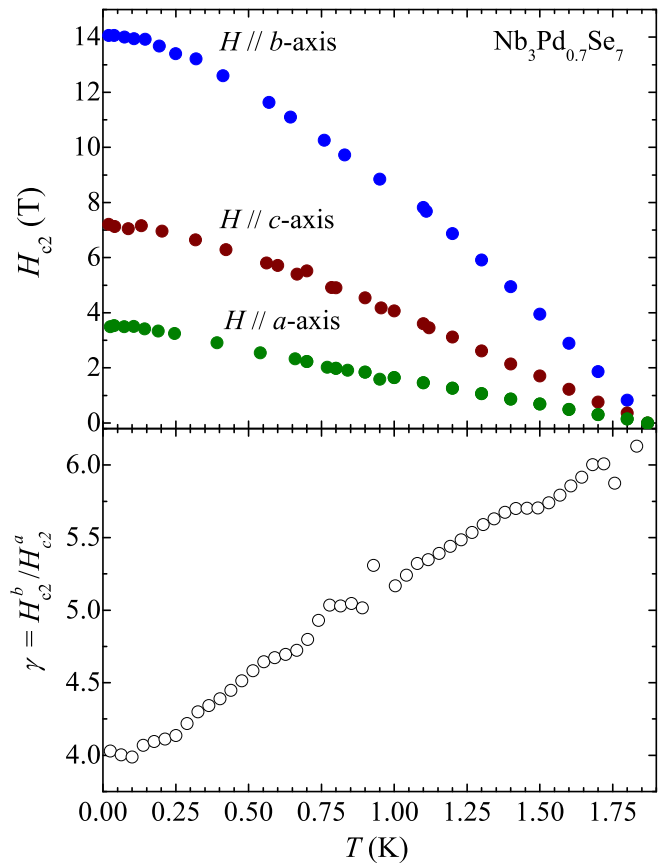


FIG. 5. (color online) Upper panel: phase boundary between superconducting and metallic states in the temperature (T) - magnetic field (H) plane for $\text{Nb}_3\text{Pd}_{0.7}\text{Se}_7$. Blue markers depict the phase-boundary for fields applied along the needle, or the b -axis of the crystal. Brown and green markers depict the phase-boundary for fields applied c -axis and a -axis, respectively. Lower panel: Anisotropy in upper-critical fields $\gamma = H_{c2}^b/H_{c2}^a$ as a function of temperature. Notice that γ is temperature-dependent as previously observed in multi-band superconductors.

$(H_p/H_o)^2$, the Pauli limiting field H_p dominates the shape of $H_{c2}(T) \propto (1 - t)^{1/2}$ even in the GL domain if $H_p < H_o$. The latter inequality is equivalent to the condition that the Maki parameter $\alpha \sim H_o/H_p > 1$ is large enough, assuring that the paramagnetic effects are essential. Shown in the upper panel of Fig. 6 are the log-log plots of our $H_{c2}(T)$ as a function of $1 - T/T_c$ where the red lines are fits to Eq. (1). As seen, for fields along the b -axis (blue markers) the fitting yields $H_p = (19 \pm 0.5)$ T and $H_o = (35 \pm 3)$ T respectively, implying a Maki parameter of 2.6 if one uses both values resulting from the fittings, or $\alpha \simeq 3.5$ if one used the experimental result 14.1 T as a tentative value for the Pauli limiting field. In any case, such large values for the paramagnetic limiting field relative to T_c would be difficult to understand for a conventional superconductor, suggesting either very strong correlations renormalizing

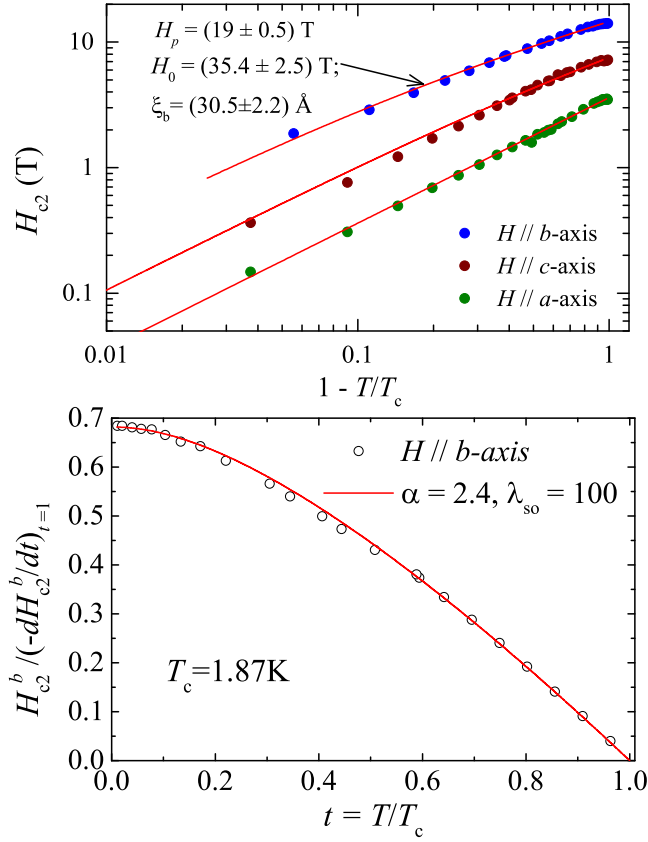


FIG. 6. (Color online) Upper panel: H_{c2} for $\text{Nb}_3\text{Pd}_{0.7}\text{Se}_7$ as a function of $1-t$, where $t = T/T_c$ for fields applied along the b -axis (blue dots), c -axis (brown dots) and a -axis (green dots). Red lines are fits to Eq. 1. Lower panel: H_{c2}^b for fields along the b -axis normalized by the linear slope at T_c and as a function of t . Red line is a fit to the WHH formalism.

H_p as seen in the heavy-fermions, or an unconventional pairing mechanism, or both. Notice that these values for α are > 1.8 the value required for the observation of the FFLO-state [27]. For the other two orientations, one obtains similar values for both H_p and H_o . The lower panel of Fig. 6 shows a fit to H_{c2}^b normalized by the slope of its linear dependence at T_c and as a function of the reduced temperature T/T_c . Red line is a fit to the Werthamer, Helfand, and Hohenberg formalism [29] with a tentative value of the Maki parameter $\alpha = 2.4$ which yields an extremely large value for the spin-orbit coupling parameter $\lambda_{so} = 100$. Although it remains unclear how reliable such a large value is, this suggests that the spin-orbit coupling plays a relevant role for this system.

To shed some light about the possible superconducting pairing mechanism in $\text{Nb}_3\text{Pd}_{0.7}\text{Se}_5$ we have performed band structure calculations to determine the geometry of the Fermi surface, the results are summarized in Fig. 7. Density functional theory calculations using Wien2K [32] with the Generalized Gradient Approximation (GGA) [33] to the exchange correlation poten-

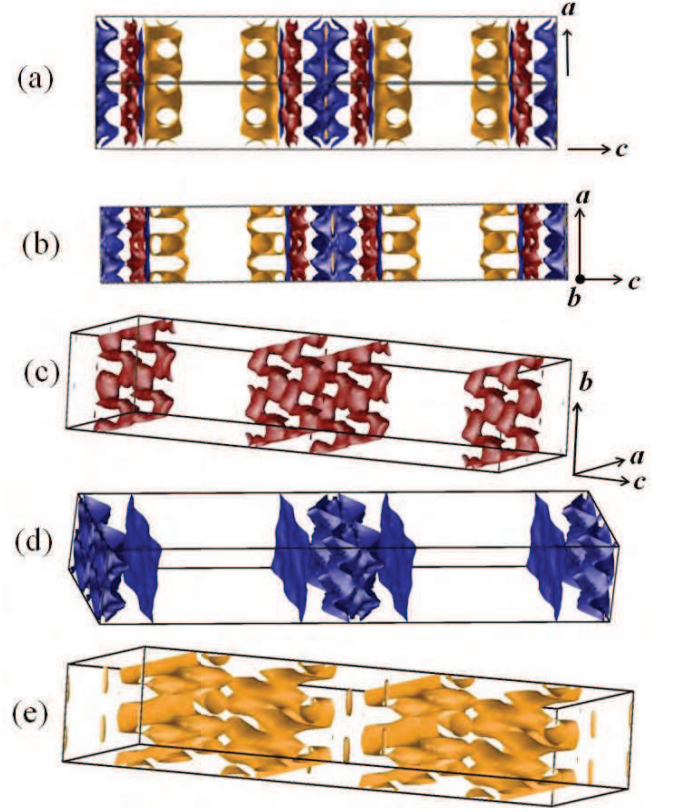


FIG. 7. (color online) (a) Top perspective of the geometry of the Fermi surface of $\text{Nb}_3\text{Pd}_{0.7}\text{Se}_7$ in a $2 \times 2 \times 2$ conventional reciprocal unit cell as obtained through DFT calculations. (b) Same as in (a) but through a lateral perspective. Maroon and blue FS sheets character, while the gold intersecting cylinders are electron-like in one direction and hole-like in the other. Notice that the FS is composed of both quasi-two-dimensional nearly cylindrical sheets as well as highly corrugated quasi-one-dimensional ones. The Q1D surfaces are extremely sensitive to the Fermi energy, which is in turn sensitive to the exact Pd content.

tial were employed to calculate the self-consistent energy eigenvalues at 16,000 k-points in the reciprocal lattice. A doubled cell with one Pd(2) atom removed was used in order to achieve a formula unit of $\text{Nb}_6\text{Pd}_{1.5}\text{Se}_{14}$, resulting in band-folding in the smaller reciprocal space cell. The FSs were calculated using the experimental lattice constants and atomic positions established in this work. The centering symmetry of space group # 12 ($C2/m$) was eliminated so that half the Pd at the $2a$ Wyckoff position could be removed, resulting in a doubled unit cell with formula $\text{Nb}_6\text{Pd}_{1.5}\text{Se}_{14}$, *i.e.* with slightly more Pd than is incorporated experimentally. As seen in Figs. 7 (c) and (d) the resulting FS is composed of quasi-2D sheets (maroon surfaces) of hole character, and a set of strongly and weakly warped Q1D (blue) sheets of hole character whose geometry is sensitive to the exact Pd content. The com-

plex 3D network itself (golden) seen in Fig. 7 (e), contains both hole- and electron-like orbits. Therefore, given that the resulting FS is composed of multiple sheets, having both electron- and hole-character, this system can indeed be classified as a multi-band superconductor. Spin-polarized calculations show that a ferromagnetic state is stable, with a small moment attributable to some Nb atoms ($0.27 \mu_B/\text{Nb}(1)$, $0.20 \mu_B/\text{Nb}(2)$) and a polarized, delocalized interstitial density. The stabilization energy is extremely small, and manipulable via variations in the Pd content indicating that the system is in proximity to magnetism. If a spin fluctuation mechanism were in play, T_c might be tunable by varying the stoichiometry as seen here.

SUMMARY

In summary, $\text{Nb}_3\text{Pd}_{0.7}\text{Se}_7$ is a new chalcogenide based multi-band superconductor, displaying extremely large upper critical-fields, i.e. comparable to those of unconventional strongly correlated heavy-fermion superconductors. The synthesis process also yields crystals of the $\text{Nb}_2\text{Pd}_x\text{Se}_5$ phase which also displays superconductivity. Both compounds display an anomalous metallic behavior, particularly for temperatures above their respective superconducting transitions which bears resemblances with the pseudogap phase of the cuprates. Such anomalous metallic behavior was not observed in $\text{Nb}_5\text{Pd}_{0.81}\text{S}_5$ which displays a considerably higher superconducting transition temperature [7]. This clearly indicates that the fraction x of Pd plays the role of a dopant, i.e. by varying its content one can, for instance, suppress non-metallic states and stabilize superconductivity as observed in the $\text{Nb}_2\text{Pd}_x\text{Se}_5$ series. Notice that this study was confined to a narrow range in x , from ~ 0.67 to $\gtrsim 0.7$ where we have shown that small variations in x or $\Delta x = 0.03$ easily suppress superconductivity in both families of compounds. Therefore, the overall behavior reported here for the $\text{Nb}_3\text{Pd}_x\text{Se}_7$ series is clearly characteristic of an underdoped regime. As we already implied within the Introduction, an anomalous metallic behavior with broad anomalies which cannot be clearly attributed to phase-transitions and which instead suggest crossovers towards new electronic regimes, makes these compounds particularly distinct from the dichalcogenides or the trichalcogenides. Notice, that in quasi-one-dimensional or quasi-two-dimensional systems such as these, both charge-density waves [34] coupling to lattice distortions, and spin-density waves [35] resulting from electronic correlations lead to sharp, first-order like anomalies in their physical properties such as the resistivity [36], in contrast to what is seen here. In fact, it would seem that these compounds are more akin to the Fe chalcogenide superconductors: for example in the $\text{Fe}_{1+y}\text{Se}_x\text{Te}_{1-x}$ series the resistivity in the metallic state

is known to display a $-\log T$ dependence above the superconducting transition which can be suppressed upon careful annealing [21].

A complex Fermi surface composed also of quasi-one-dimensional sheets, interplay of superconductivity with an anomalous metallic state, extremely high upper critical fields coupled to multi-band behavior, suggest an unconventional pairing symmetry.

ACKNOWLEDGEMENT

L. B. is supported by DOE-BES through award DE-SC0002613. T. B. and T. S. are supported by DOE-BES through award DE-SC0008832, and by FSU. Funding for M.D.J. was provided by the Office of Naval Research (ONR) through the Naval Research Laboratory's Basic Research Program. The NHMFL is supported by NSF through NSF-DMR-0084173 and the State of Florida.

Appendix: Parameters of $\text{Nb}_2\text{Pd}_{0.67}\text{Se}_5$ and $\text{Nb}_3\text{Pd}_{0.7}\text{Se}_7$ as derived from the X-ray refinements

Compound	$\text{Nb}_2\text{Pd}_{0.67}\text{Se}_5$	$\text{Nb}_3\text{Pd}_{0.70}\text{Se}_7$
Space group	$C2/m$	$C2/m$
a (Å)	12.8325(7)	12.7965(6)
b (Å)	3.39327(18)	3.40591(17)
c (Å)	15.3859(8)	21.0370(13)
β (°)	101.471(5)	95.530(5)
α, γ (°)	90.0	90.0
Z	4	4
V (Å ³)	656.59(6)	912.60(8)
$d_{\text{cal.}}$ (g/cm ³)	6.599	6.590
T (K)	298	298
Range (°)	$3.24 < \theta$	$2.92 < \theta$
	< 66.41	< 45.00
Reflections	6162	4170
Parameters refined	52	70
Goodness-of-fit	1.0046	1.1150

TABLE I. Crystallographic parameters as extracted from single-crystal x -ray refinements for two typical crystals resulting from the synthesis process.

* balicas@magnet.fsu.edu

[1] T. M. McQueen, Q. Huang, V. Ksenofontov, C. Felser, Q. Xu, H. Zandbergen, Y. S. Hor, J. Allred, A. J. Williams, D. Qu, J. Checkelsky, N. P. Ong, and R. J. Cava, Phys. Rev. B **79**, 014522 (2009).

Nb₂Pd_{0.67}Se₅

Atom	Site	Occupation	x	y	z	U_{eq}
Nb1	4i	1	0.07595(4)	1/2	0.17999(3)	0.0099
Nb2	4i	1	0.15288(4)	0	0.37854(3)	0.0078
Pd1	2a	1	0	0	0	0.0124
Pd2	2c	0.348(5)	0	0	1/2	0.0117
Se1	4i	1	0.35036(5)	0	0.48914(3)	0.0098
Se2	4i	1	0.25374(4)	1/2	0.29566(3)	0.0086
Se3	4i	1	0.17536(5)	0	0.09778(4)	0.0106
Se4	4i	1	0.42303(5)	1/2	0.13214(4)	0.0104
Se5	4i	1	0.50041(4)	0	0.32346(4)	0.0091

Nb₃Pd_{0.70}Se₇

Atom	Site	Occupation	x	y	z	U_{eq}
Nb1	4i	1	0.05848(5)	1/2	0.12765(3)	0.0105
Nb2	4i	1	0.11676(5)	0	0.26968(3)	0.0083
Nb3	4i	1	0.16833(5)	1/2	0.41178(3)	0.0071
Pd1	2a	1	0	0	0	0.0126
Pd2	2d	0.393(5)	0	1/2	1/2	0.0109
Se1	4i	1	0.35141(6)	1/2	0.49292(3)	0.0089
Se2	4i	1	0.16650(6)	0	0.06770(4)	0.0108
Se3	4i	1	0.40985(6)	1/2	0.09657(4)	0.0103
Se4	4i	1	0.22426(6)	1/2	0.20964(4)	0.0091
Se5	4i	1	0.28063(6)	0	0.35319(3)	0.0078
Se6	4i	1	0.47084(6)	0	0.23370(3)	0.0083
Se7	4i	1	0.02204(6)	0	0.37263(3)	0.0088

TABLE II. Single-Crystal X-ray diffraction collection and refinement: positional data for Nb₂Pd_{0.67}Se₅ and Nb₃Pd_{0.70}Se₇.

- [2] M. Burrard-Lucas, D. G. Free, S. J. Sedlmaier, J. D. Wright, S. J. Cassidy, Y. Hara, A. J. Corkett, T. Lancaster, P. J. Baker, S. J. Blundell, S. J. Clarke, *Nat. Mat.* **12**, 15, (2013).
- [3] A. -m. Zhang, T. -l. Xia, K. Liu, W. Tong, Z. -r. Yang, and Q. -m. Zhang, *Sci. Rep. (UK)* **3**, 1216 (2013).
- [4] Y. Lubashevsky, E. Lahoud, K. Chashka, D. Podolsky and A. Kanigel, *Nat. Phys.* **8**, 309 (2012).
- [5] M. Yi, D. H. Lu, R. Yu, S. C. Riggs, J. -H. Chu, B. Lv, Z. K. Liu, M. Lu, Y. -T. Cui, M. Hashimoto, S.K. Mo, Z. Hussain, C. W. Chu, I. R. Fisher, Q. Si, and Z. -X. Shen, *Phys. Rev. Lett.* **110**, 067003 (2013).
- [6] A. F. May, M. A. McGuire, H. Cao, I. Sergueev, C. Cantoni, B. C. Chakoumakos, D. S. Parker, and B. C. Sales, *Phys. Rev. Lett.* **109**, 077003 (2012).
- [7] Q. Zhang, G. Li, D. Rhodes, A. Kiswandhi, T. Besara, B. Zeng, J. Sun, T. Siegrist, M. D. Johannes, and L. Balicas, *Sci. Rep. (UK)* **3**, 1446 (2013).
- [8] X. H. Chen, T. Wu, G. Wu, R. H. Liu, H. Chen, D. F. Fang, *Nature* **453**, 761 (2008);
- [9] A. S. Sefat, R. Y. Jin, M. A. McGuire, B. C. Sales, D. J. Singh, D. Mandrus, *Phys. Rev. Lett.* **101**, 117004 (2008).
- [10] G. F. Chen, Z. Li, G. Li, W. Z. Hu, J. Dong, J. Zhou, Z. D. Zhang, P. Zheng, N. L. Wang, J. L. Luo, *Chinese Phys. Lett.* **25**, 3403 (2008).
- [11] For recent results see, V. G. Tissen, M. R. Osorio, J. P. Brison, N. M. Nemes, M. García-Hernandez, L. Cario, P. Rodière, S. Vieira, and H. Suderow, *Phys. Rev. B* **87**, 134502 (2013).
- [12] For recent results see, T. Ritschel, J. Trinckauf, G. Garbarino, M. Hanfland, M. v. Zimmermann, H. Berger, B. Büchner, and J. Geck, *Phys. Rev. B* **87**, 125135 (2013).
- [13] See, for example, A. A. Sinchenko, and P. Monceau, *Phys. Rev. B* **87**, 045105 (2013) and references therein.
- [14] A. M. Gabovich, A. I. Voitenko, and M. Ausloos, *Phys. Rep.* **367**, 583 (2002).
- [15] B. W. Pfalzgraf, and H. Spreckels, *J. Phys. C: Solid State Phys.* **20**, 4359 (1987).
- [16] D. Sanchez, A. Junod, J. Muller, H. Berger, F. Levy, *Physica B* **204**, 167 (1995); N. Toyota, H. Nakatsuji, K. Noto, A. Hoshi, N. Kobayashi, Y. Muto, Y. Onodera, *J. Low Temp. Phys.* **25**, 485 (1976).
- [17] D. A. Keszler and J. A. Ibers, *J. Am. Chem. Soc.* **107**, 8119 (1985).
- [18] See, for example, R. H. Liu, G. Wu, T. Wu, D. F. Fang, H. Chen, S. Y. Li, K. Liu, Y. L. Xie, X. F. Wang, R. L. Yang, L. Ding, C. He, D. L. Feng, and X. H. Chen, *Phys. Rev. Lett.* **101**, 087001 (2008).
- [19] T. Timusk, and B. Statt, *Rep. Prog. Phys.* **62**, 61 (1999).
- [20] H. Takagi, B. Batlogg, H. L. Kao, J. Kwo, R. J. Cava, J. J. Krajewski, and W. F. Peck, Jr. *Phys. Rev. Lett.* **69**, 2975 (1992).
- [21] T. Gebre, G. Li, J. B. Whalen, B. S. Conner, H. D. Zhou, G. Grissonnanche, M. K. Kostov, A. Gurevich, T. Siegrist, and L. Balicas, *Phys. Rev. B* **84**, 174517 (2011).
- [22] A. Bianchi, R. Movshovich, C. Capan, P. G. Pagliuso, and J. L. Sarrao, *Phys. Rev. Lett.* **91**, 187004 (2003).
- [23] J. P. Brison *et al.*, *Physica C* **250**, 128 (1995); J. P. Brison *et al.*, *Physica B* **199**, 70 (1994).
- [24] K. Okuda, M. Kitagawa, T. Sakakibara, and M. Date, *J. Phys. Soc. Jpn.* **48**, 2157 (1980).
- [25] B. T. Matthias, T. H. Geballe, S. Geller, and E. Corenzwit, *Phys. Rev.* **95**, 1435 (1954); R. M. Scanlan, A. P. Malozemoff, and D. C. Larbalestier, *P. IEEE* **92**, 1639 (2004).
- [26] J. -F. Mercure, A. F. Bangura, Xiaofeng Xu, N. Wakeham, A. Carrington, P. Walmsley, M. Greenblatt, and N. E. Hussey *Phys. Rev. Lett.* **108**, 187003 (2012).
- [27] L. W. Gruenberg and L. Gunther, *Phys. Rev. Lett.* **16**, 996 (1966).
- [28] A. Gurevich, *Phys. Rev. B* **82**, 184504 (2010).
- [29] N. R. Werthamer, E. Helfand, and P. C. Hohenberg, *Phys. Rev.* **147**, 295 (1966).
- [30] H. Q. Yuan, J. Singleton, F. F. Balakirev, S. A. Baily, G. F. Chen, J. L. Luo, N. L. Wang, *Nature* **457**, 565 (2009).
- [31] A. Yamamoto, J. Jaroszynski, C. Tarantini, L. Balicas, J. Jiang, A. Gurevich, D. C. Larbalestier, R. Jin, A. S. Sefat, M. A. McGuire, B. C. Sales, D. K. Christen, D. Mandrus, *Appl. Phys. Lett.* **94**, 062511 (2009).
- [32] P. Blaha, K. Schwarz, P. Sorantin, and S. B. Trickey, *Comput. Phys. Commun.* **59**, 399 (1990); K. Schwarz and P. Blaha, *Comput. Mater. Sci.* **28**, 259 (2003).
- [33] J. P. Perdew, S. Burke, and M. Ernzerhof, *Phys. Rev. Lett.* **77**, 3865 (1996).
- [34] G. Grüner, *Rev. Mod. Phys.* **60**, 1129 (1988).
- [35] G. Grüner, *Rev. Mod. Phys.* **66**, 1 (1994).
- [36] See, for example, N. Biškup, S. Tomić, and D. Jérôme, *Phys. Rev. B* **51**, 17972 (1995).